Electronics and Electrical Engineering

AIMS Electronics and Electrical Engineering, 7(2): 156–170.
DOI: 10.3934/electreng.2023009
Received: 26 January 2023
Revised: 22 March 2023
Accepted: 30 March 2023
Published: 08 May 2023

http://www.aimspress.com/journal/ElectrEng

Research article

Adaptive online auto-tuning using Particle Swarm optimized PI controller with time-variant approach for high accuracy and speed in Dual Active Bridge converter

Suliana Ab-Ghani[1,*], Hamdan Daniyal[1], Abu Zaharin Ahmad[1], Norazila Jaalam[1], Norhafidzah Mohd Saad[1], Nur Huda Ramlan[1] and Norhazilina Bahari[2]

[1] FTKEE, Universiti Malaysia Pahang, 26600 Pekan, Pahang, Malaysia
[2] FKE, Universiti Teknikal Malaysia Melaka, Hang Tuah Jaya, 76100 Durian Tunggal, Melaka, Malaysia

* **Correspondence:** Email: suliana@ump.edu.my; Tel: +6-019-753-4645.

Abstract: Electric vehicles (EVs) are an emerging technology that contribute to reducing air pollution. This paper presents the development of a 200 kW DC charger for the vehicle-to-grid (V2G) application. The bidirectional dual active bridge (DAB) converter was the preferred fit for a high-power DC-DC conversion due its attractive features such as high power density and bidirectional power flow. A particle swarm optimization (PSO) algorithm was used to online auto-tune the optimal proportional gain (K_P) and integral gain (K_I) value with minimized error voltage. Then, knowing that the controller with fixed gains have limitation in its response during dynamic change, the PSO was improved to allow re-tuning and update the new K_P and K_I upon step changes or disturbances through a time-variant approach. The proposed controller, online auto-tuned PI using PSO with re-tuning (OPSO-PI-RT) and one-time (OPSO-PI-OT) execution were compared under desired output voltage step changes and load step changes in terms of steady-state error and dynamic performance. The OPSO-PI-RT method was a superior controller with 98.16% accuracy and faster controller with 85.28 s^{-1} average speed compared to OPSO-PI-OT using controller hardware-in-the-loop (CHIL) approach.

Keywords: electric vehicles; dual active bridge; particle swarm optimization; online auto-tuning; time variant

1. Introduction

Global warming is a radically aggravating phenomenon due to many causes. One such cause is the burning of fossil fuels in line with the growing of energy consumption. Among the many approaches that have been implemented to mitigate the environmental problems, power electronics (PE), which is efficient in deploying energy, has been identified as the key player in producing green energy [1]. Progression of renewable energy (RE) and smart microgrid have instigated the growth of PE applications such as electric vehicles (EVs) and energy storage units [2].

The development of EVs was predicted to grow rapidly as have the features of clean technology [3]. Moreover, the implementation of RE sources in EVs has significantly reduced the dependency on fossil fuels [4]. Plug-in Hybrid Electric Vehicles (PHEV) is an example of a vehicle-to-grid (V2G), which is built-in with battery pack and grid connection [4,5]. Having said that, there are two types of EV chargers, namely the on-board charger and off-board charger, the AC and DC types, respectively [6]. This study, however, designed a system to be compatible with the off-board DC charger of CHAdeMO 1.2 type standard with 200 kW rated power and 400 A maximum current [7]. This study only considers the bidirectional DC-DC converter as depicted in Figure 1.

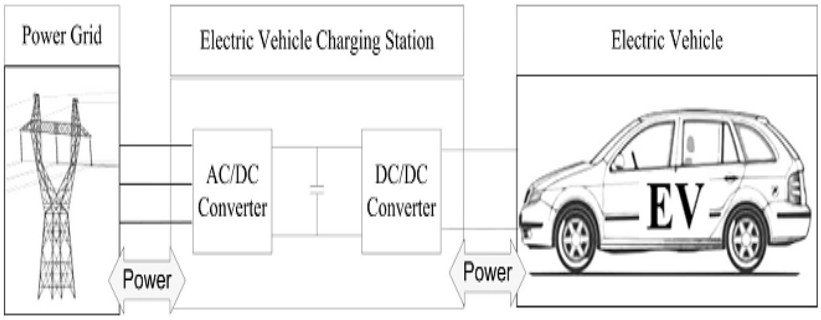

Figure 1. Overview of power flow in V2G [8] and the DC-DC converter.

The bidirectional power flow in DC-DC converter acts as an interface between DC high voltage bus and EVs battery. The bidirectional power flow can be classified into a non-isolated and isolated structure. Based on the variable voltage conversion ratio and safety benefits, isolated configuration is usually chosen instead of the non-isolated structure [9,10]. Having said that, the dual active bridge (DAB) isolated DC-DC converter is most preferred in the energy storage system (ESS) applications [11,12].

DAB converter was introduced in the 1990s [13]. In DAB there are bidirectional power flow features that are it capable of storing energy during charging and the energy is sent back to the grid during the discharging mode [4,14]. Apart from that, the promising soft switching, high efficiency, high power density, simple control strategy and galvanic isolation of the DAB DC-DC converter made it popular recently [15,16].

The DAB system employs many optimization techniques. Among the available techniques, the particle swarm optimization (PSO) algorithm is the most widely accepted due to fewer parameters, high speed of convergence time and simple mathematical equation [17,18] compared to Lagrange Multiplier [19] and analytical method based on Karush–Kuhn–Tucker [20]. Several studies have proposed an offline method to determine optimal phase-shift angle, ϕ using PSO to minimize

reactive power [21] and current stress [22]. Despite the advantages of the offline method such as reducing the computing cost [23], its implementation in real time has a downside whereby the parameter or setting needs to be adjusted in the prepared lookup table if there are any changes. Meanwhile, online optimization method in DAB using an analytical method based on global optima technique was developed to minimize backflow power [24] and root mean square (RMS) current [25].

On the other hand, the proportional-integral (PI) controller is a linear controller that is widely used in various applications, including power electronic applications due to its simple design and effectiveness [18]. PI controller is also used to regulate the output voltage in the DAB system. However, the PI controller tuning process has demerits in term of time consuming and stability guaranteed because of the trial-and-error method used and it only delivers satisfactory performance for narrow operating range [26]. Hence, PSO is the most preferred method for tuning and obtaining the optimal PI parameters [27,28,29] that results in less overshoot, low total harmonic distortion and improves the fast response.

Even though the offline and online tuning of PI using PSO have already been researched, the online auto-tuned PI controller using PSO algorithm have not been evaluated yet in DAB DC-DC converter in analyzing steady-state error, e_{SS} and transient response in order to evaluate the system accuracy and speed's controller, respectively. Hence, this paper presents the development of DAB DC-DC converter using online auto-tuned by re-tuning features through the PSO-PI method. This method is crucial in the DAB system, especially in EV or transportation applications due to the system's robustness and high dynamic response [30,31]. The re-tuning method was introduced to address the issue of the fixed gains restriction, which provided the same responses to the applied changes in dynamic system [32]. Moreover, recent research has incorporated artificial intelligence substantially in the use of EVs, such as voltage control strategy based on deep reinforcement learning [33] and multiagent reinforcement learning method [34]. Yet, the PSO algorithm is still relevant due to less computational methods and is efficient to be embedded in the system environments [18].

The online auto-tuned PSO-PI with re-tuning approach (OPSO-PI-RT) based on the single-phase-shift (SPS) modulation is proposed in this study and is compared with online auto-tuned PSO-PI with a one-time execution (OPSO-PI-OT) technique. The SPS modulation was chosen due to its competition efficient feature for the system design.

Section II of this paper discusses the DAB system and SPS control. Section III outlines the overview of the PSO and how PI is tuned using the stochastic optimization. The setup of Hardware-in-the-Loop (HIL) is detailed in Section IV. Meanwhile, the experimental results of the e_{SS} and dynamic performance of the four methods are analyzed in Section V. Lastly, Section VI concludes this study.

2. Switching mode analysis of SPS control

The DAB, as depicted in Figure 2, is a DC-DC converter of two active bridges. Both bridges are interfaced through a high frequency transformer. The leakage inductance, L_k, is the main element of energy transferring in the DAB. The equivalent topology of DAB converter is illustrated in Figure 3, where V_1 is the voltage at primary side, V_2 is the voltage at secondary side, I_{Lk} is the current of leakage inductance and V_{Lk} is the voltage of leakage inductance. The pulse width modulation (PWM)

switching at each bridge is set to 50% of the duty cycle to enable both bridges to produce a symmetrical square-wave pulse with a ϕ value between the bridges. A constant switching frequency is used in the design.

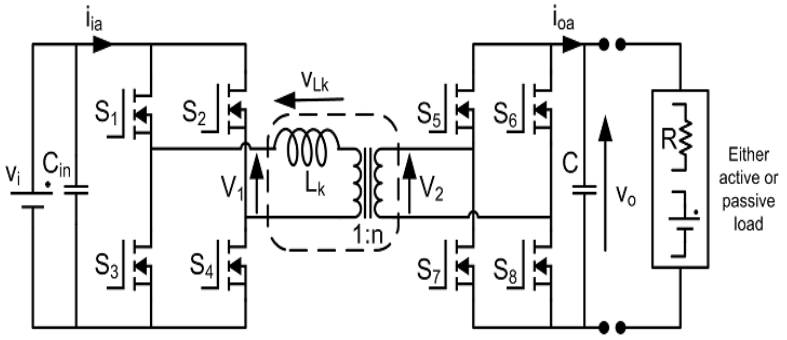

Figure 2. Basic schematic of DAB converter [39].

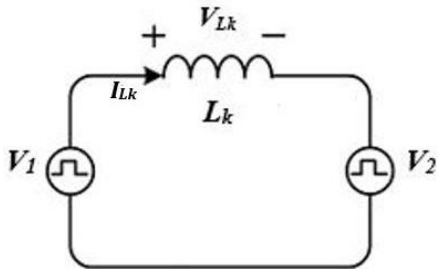

Figure 3. Equivalent circuit of DAB converter.

SPS is one of the modulation strategies that have been applied in DAB. It is the simplest strategy that produces high efficiency when operated under narrow voltage variations, where voltage conversion ratio, *k* is close to one [36]. Despite the improvement of phase-shift modulation, such as extended phase-shift (EPS), dual phase-shift (DPS) and triple phase-shift (TPS), the SPS is still preferred as it is easy to implement and reliable [30,37,38].

SPS only needs to control one ϕ to control the magnitude and direction of power flow in DAB. The primary side leads to the second part in a forward direction and conversely in reverse power flow. The power transmission of DAB can be obtained using (1), where T_s denotes switching the interval. Following mathematical manipulations, the power flow can be expressed as (3), in which V_i represents input voltage, V_o output voltage, *n* transformer turns ratio and f_s switching frequency.

$$P = \frac{1}{T_s}\int_{t_0}^{t_4} V_1(t) i_{Lk}(t) dt \tag{1}$$

$$P = \frac{1}{2\pi}\int_{0}^{2\pi} V_1(t) i_{Lk}(t) dt \tag{2}$$

$$P = \frac{nV_i V_o \phi_{12}}{2\pi f_s L_k}\left(1 - \frac{\phi_{12}}{\pi}\right);\ \phi_{12} = \phi_1 - \phi_2 \tag{3}$$

The maximum power can be calculated as (4), which occurs when ϕ is 90 °($\frac{\pi}{2}$). The transformer turns ratio, *n* and voltage conversion ratio, *k* can be calculated using (5) and (6) respectively, where N_P and N_S represent the primary turn and secondary turn of the transformer correspondingly.

$$P_{max} = \frac{nV_iV_o}{8f_sL_k} \tag{4}$$

$$n = \frac{N_P}{N_S} \tag{5}$$

$$k = \frac{nV_o}{V_i} \tag{6}$$

Figure 4 indicates the square waveform at each bridge and leakage inductance voltage, V_{LK} when V_1 = 750 V and V_2 = 500 V with maximum ϕ at 90 °. Only one ϕ need to be controlled in this system since the SPS modulation is used.

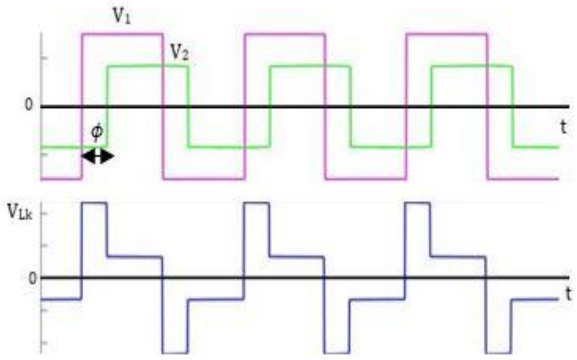

Figure 4. Square waveform at both bridges and leakage inductance voltage. In the forward direction, V_1 (primary bridge) leads to V_2 (secondary bridge).

3. Proposed OPSO-PI-RT controller

3.1. Particle swarm optimization

PSO is a stochastic algorithm based on the social behavior of bird flocking or fish schooling that was introduced in 1995 [39]. This swarm intelligence conducts a search process using a group of particles. Each particle represents a candidate solution to the given problem. Particles set with initial parameters will explore and exploit iteratively following the objective function until the desired outcome is achieved. In each iteration, the particles will update the particle best, P_{best}, then global best, G_{best} will be selected from the best of P_{best} solution. The velocity and position of the particles involved are adjusted using (7) and (8) respectively.

$$v_i(k+1) = wv_i(k) + c_1r_1\left[P_{best_i} - x_i(k)\right] + c_2r_2[G_{best} - x_i(k)] \tag{7}$$

$$x_i(k+1) = x_i(k) + v_i(k+1) \tag{8}$$

where w is the inertia weight, c_1 and c_2 are the acceleration coefficient, r_1 and r_2 are the random number between 0 to 1, P_{best} is the personal best position of particle i, G_{best} is best position of the particles and k represents the iteration number.

3.2. Online auto-tuned PI using PSO algorithm

In the proposed method, PI controller is used to regulate the ϕ as to control the desired V_o. Hence,

optimal proportional gain (K_P) and integral gain (K_I) values using PSO will produce the suitable ϕ as to yield the desired V_o. The block diagram of the proposed method is illustrated in Figure 5.

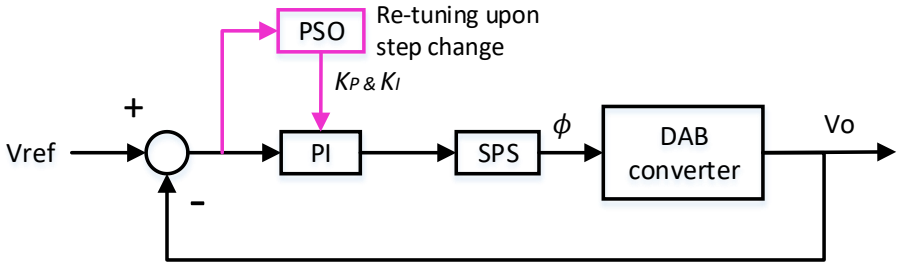

Figure 5. Block diagram of the proposed OPSO-PI-RT method.

The objective function is defined by the minimum root mean square error (RMSE) as shown in (9).

$$RMSE_{min} = \sqrt{\frac{1}{N}\sum_{i=1}^{N}(V_{ref} - V_o)^2} \tag{9}$$

The PSO parameter of w, c_1, c_2, r_1 and r_2 in the proposed method are fixed values. The three particles which represent the three pairs of K_P and K_I are used during the search process through time variant [40,41] as illustrated in Figure 6. Each particle is limited to 0.5 ms for each iteration. In the first iteration, the initial K_P and K_I values evaluate the objective function using (9). The fitness values of each particle are represented by the minimum RMSE of the DAB system. The K_P and K_I values with the best fitness values will represent P_{best} for each particle. Then, the G_{best} values were selected from the best fitness values of P_{best}, with least minimum RMSE. This is followed by the new velocity and position of particles that are updated using (7) and (8) correspondingly. The new K_P and K_I produced the right ϕ as to generate the gate signal to all eight switches (S_1 to S_8) in trying to regulate the V_o. In the second iteration, the new P_{besti} is compared with the old P_{besti}, whereby a new G_{best} is updated accordingly. Then, the velocity and position are also updated based on updated values. This process is repeated continuously until all the particles are converged at certain values. Finally, the appropriate ϕ is obtained from the optimal values of K_P and K_I, where the DAB system generates the desired output with minimum e_{SS} voltage.

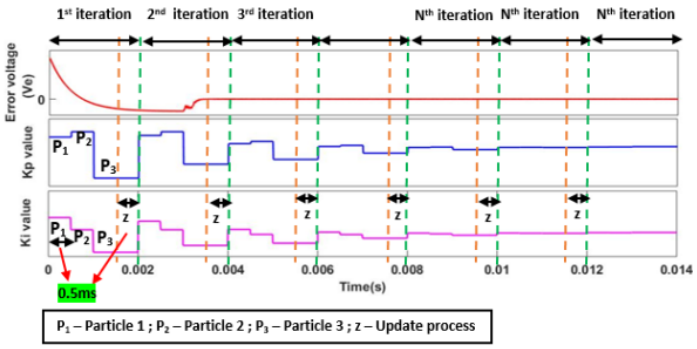

Figure 6. Overview of time-variant approach in OSO-PI-RT method.

On the other hand, the system of the proposed method is updated with reset features, whereby the K_P and K_I values change according to the new load or desired V_o. When the step changes occurred, PSO algorithm was triggered to allow the re-tuning process. Then, the particles are initialized again at the initial position when all reset requirements, such as all particles must be in convergence state; error voltage, V_e must be greater and equal than certain values and all fitness values for each particle must converge with each other satisfactorily. Those requirements are vital to avoid the PSO from performing sudden re-tuning at the initial iteration while *Ve* is still large.

All particles continued with the optimization process as reflected in the new condition, with these procedures being iterated several times until reaching the termination criterion by assuming that no step-changes occurred again. However, if the step-change occurred for the second time before the termination and fulfilled the re-tuning principles, the re-tuning process will be repeated to regulate the output as desired. Then, the new K_P and K_I will be optimized following the previous steps to conceive a DAB system with minimum e_{SS}. Therefore, with re-tuning ability, PSO can make new searches to adapt with new conditions to regulate new V_o. Figure 7 and Figure 8 depict the flowchart and overview of the working re-tuning in the proposed method, respectively.

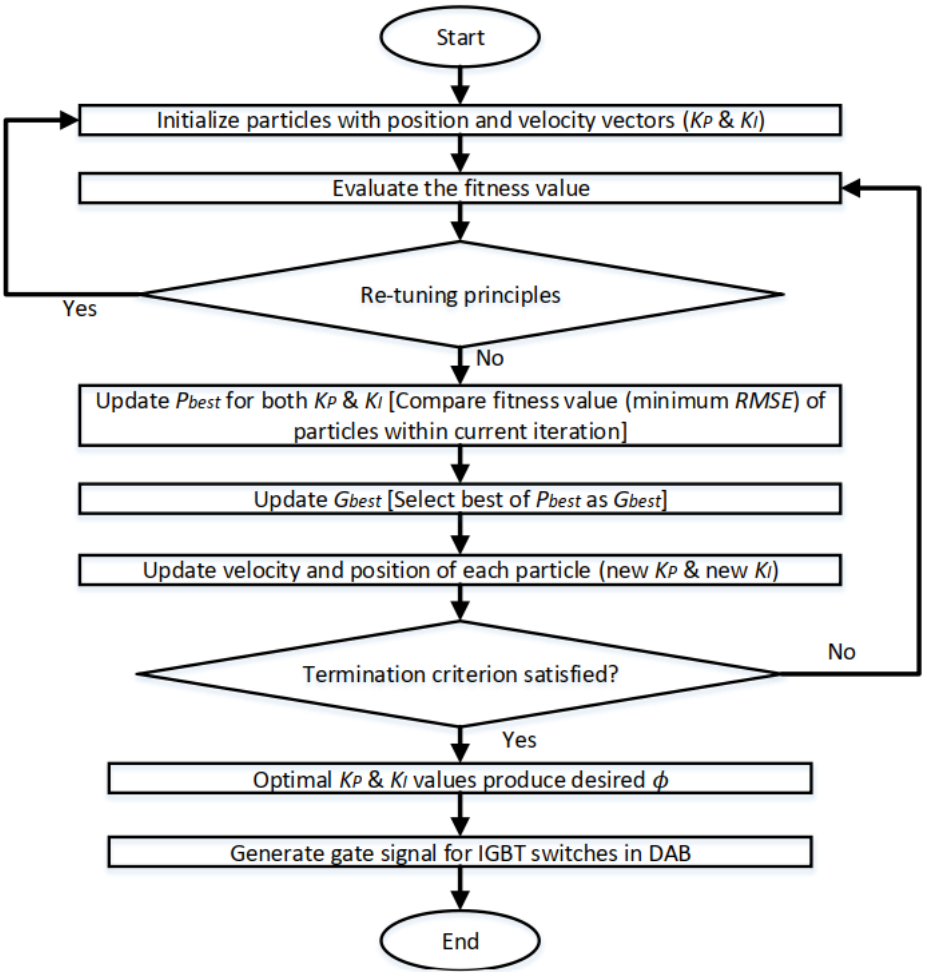

Figure 7. Flowchart of OPSO-PI-RT method.

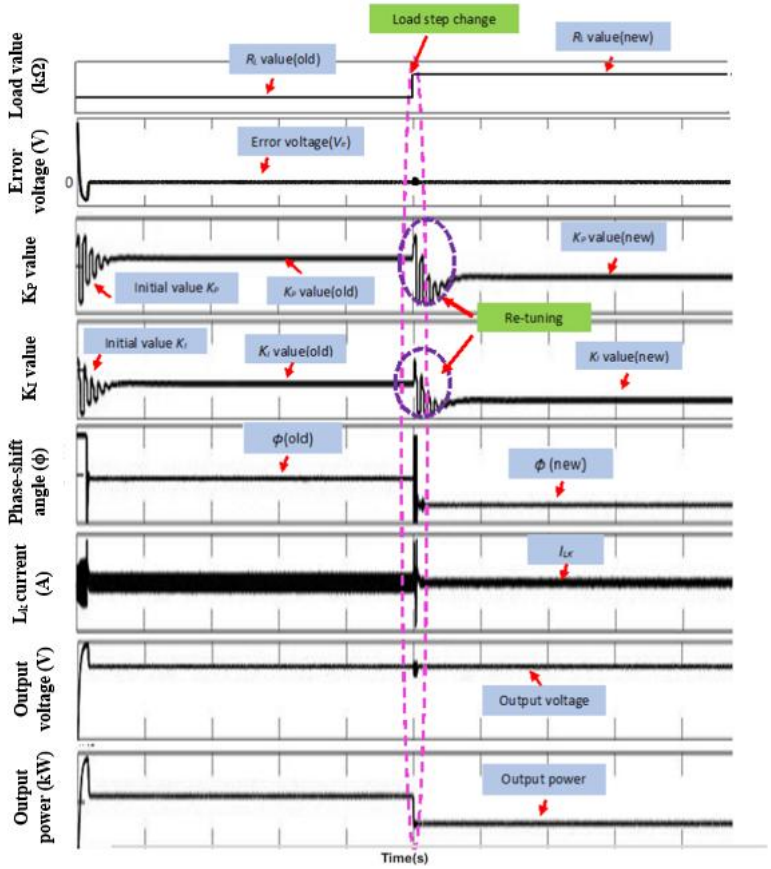

Figure 8. Overview of re-tuning in the proposed OSO-PI-RT method.

Meanwhile, the one-time execution method (OPSO-PI-OT) follows a similar concept to OPSO-PI-RT. However, the difference lies during the step change or disturbances, where the K_P and K_I values in OPSO-PI-OT maintain and try to regulate the desired output with the old optimal PI values.

4. Setup of Hardware-In-The-Loop

In real-time implementation, the algorithms of the DAB controller for all methods were implemented using Texas Instrument F28335 DSP card control. The hardware emulator, Typhoon-HIL 402 was used to develop the power circuit of the DAB converter. Moreover, a built-in field-programmable gate array (FPGA) in the Typhoon enables the modelling system to perform under a real-time form. Figure 9 presents the controller hardware-in-the-loop (CHIL) setup for a 200 kW DAB system designed using the parameters tabulated in Table 1. The V_o from DAB system in Typhoon-HIL is fed to the DSP card controller.

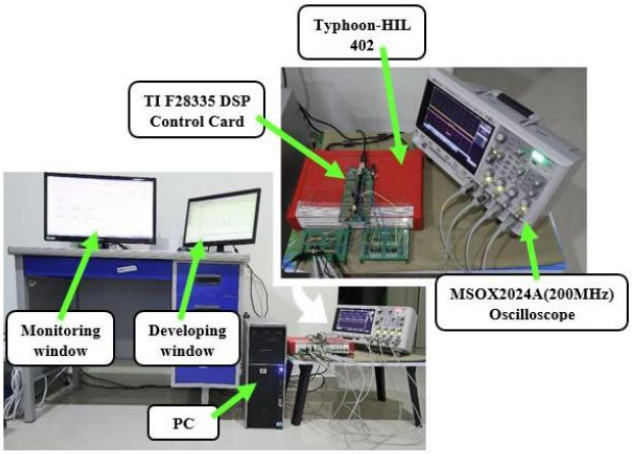

Figure 9. CHIL set-up of the DAB converter.

Table 1. Design parameters of 200 kW DAB system.

Components	Values
Transformer turns ratio, n	2 :1
Rated power, P_{max}	200 kW
Input voltage, V_i	750 V
Output voltage, V_o	500 V
Leakage inductance, L_k	24 μH
Switching frequency, f_s	20 kHz

The controller of the PSO algorithm and PI controller was implemented in MATLAB/Simulink (MATLAB Support Package for TI C2000 library) and loaded into the DSP board. Then, the ϕ that was produced was sent to the gate signal of the switches in DAB circuit through enhanced pulse width modulator (ePWM) module. The deadtime was set to 0.6 μs and the DAB converter operated at a fixed switching frequency of 20 kHz.

5. Results

5.1. Steady-state performance

Table 2 presents the steady-state and transient response performances of the DAB converter during load step-change at 270 V, 375 V and 420 V. The e_{SS} is measured during the steady-state response after applying the disturbance or step change to the system. The steady-state performance was initially evaluated by applying the load-step change during half load (100 kW) to full load (200 kW) condition. When the load was stepped-up from 100 kW to 200 kW at 270 V as depicted in Figure 10, the e_{SS} of the OPSO-PI-OT has a higher percentage of e_{SS} with 1.47% compared to OPSO-PI-RT. The proposed OPSO-PI-RT method yielded the least e_{SS} with 1.39%, where it was 5.44% more accurate than OPSO-PI-OT. Besides, the best accuracy is exhibited by OPSO-PI-RT when the load was stepped at 375 V, where the accuracy was 5.56% superior to OPSO-PI-OT as illustrated in Figure 11. There is just a slight difference in values of e_{SS} between OPSO-PI-OT and OPSO-PI-RT

when the load was changed at 420 V, which OPSO-PI-RT only has 0.6% best performance than OPSO-PI-OT.

Table 2. Result comparison of OPSO-PI-RT and OPSO-PI-OT controller.

Load Step-change	V_{ref} (V)	Average e_{SS} (%)		Average settling time (ms)	
		OPSO-PI-OT	OPSO-PI-RT	OPSO-PI-OT	OPSO-PI-RT
100kW to 200kW	270	1.47	1.39	15.80	15.60
	375	1.44	1.36	13.70	13.20
	420	1.66	1.65	9.50	10.10
150kW to 70kW	270	4.13	3.20	10.50	10.05
	375	1.54	1.57	9.90	10.80
	420	3.84	1.70	11.10	10.60

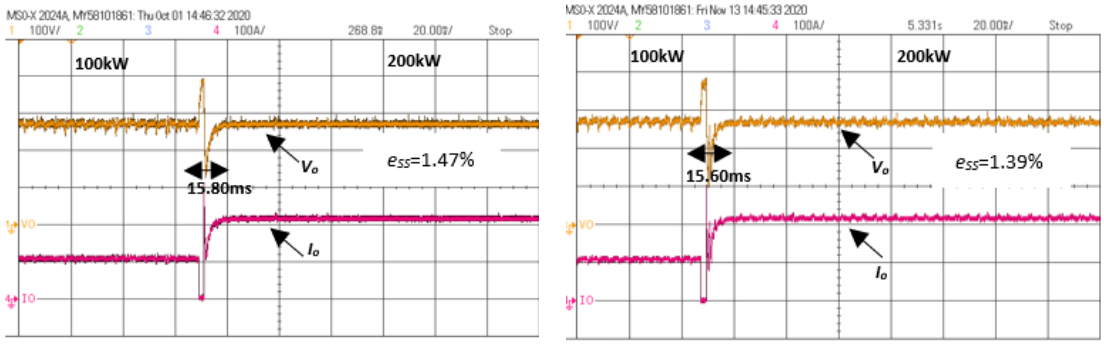

(a) (b)

Figure 10. Output waveform when the load step-up from 100 kW to 200 kW at 270 V with k = 0.72 (a) OPSO-PI-OT (b) OPSO-PI-RT (V_o: 100 V/div, I_o: 100 V/div; Time: 20 ms/div).

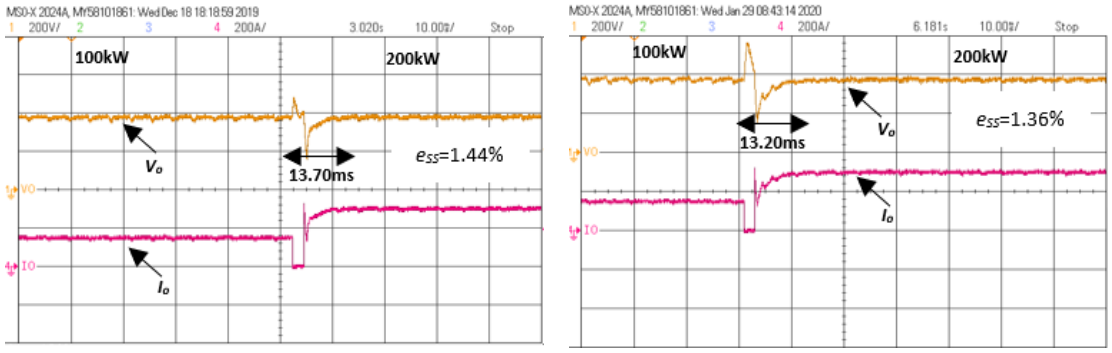

(a) (b)

Figure 11. Output waveform when the load step-up from 100 kW to 200 kW at 375 V with k = 1.00 (a) OPSO-PI-OT (b) OPSO-PI-RT (V_o: 200 V/div, I_o: 200 V/div; Time: 10 ms/div).

When the load was stepped-down from 150 kW to 70 kW at 270 V (k = 0.72), as presented in

Figure 12, the proposed OPSO-PI-RT exhibited 22.52% better performance by producing the smaller ripple voltage with 3.20% of e_{SS} relative to OPSO-PI-OT that produce 4.13% of e_{SS}. As shown in Figure 13, the OPSO-PI-RT has a tremendous performance at 420 V by producing 55.73% better accuracy than OPSO-PI-OT. With that percentage, it shows that the tuned optimal K_P and K_I values at 150 kW in the OPSO-PI-OT method are not the ideal values for the 70 kW system. Thus, it shows the significant advantages of the proposed OPSO-PI-RT that allows K_P and K_I values to update continuously according to the changes and it can eliminate more ripple voltage compared to OPSO-PI-OT.

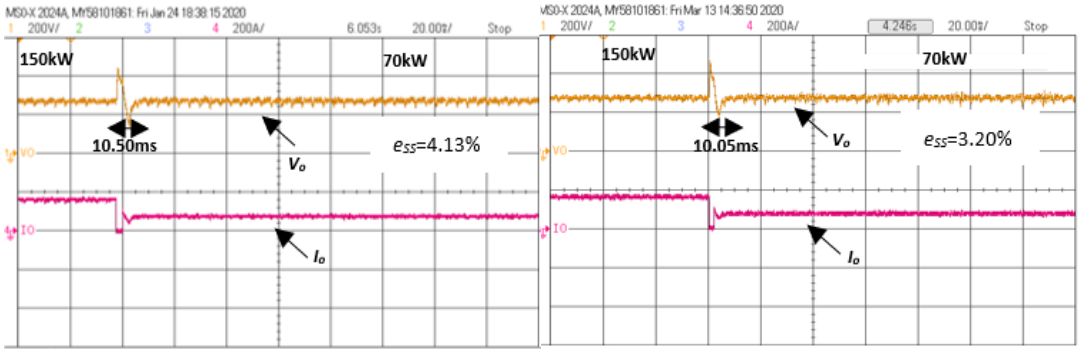

(a) (b)

Figure 12. Output waveform when the load step-down from 150 kW to 70 kW at 270 V with k = 0.72 (a) OPSO-PI-OT (b) OPSO-PI-RT (V_o: 200 V/div, I_o: 200 V/div; Time: 20 ms/div).

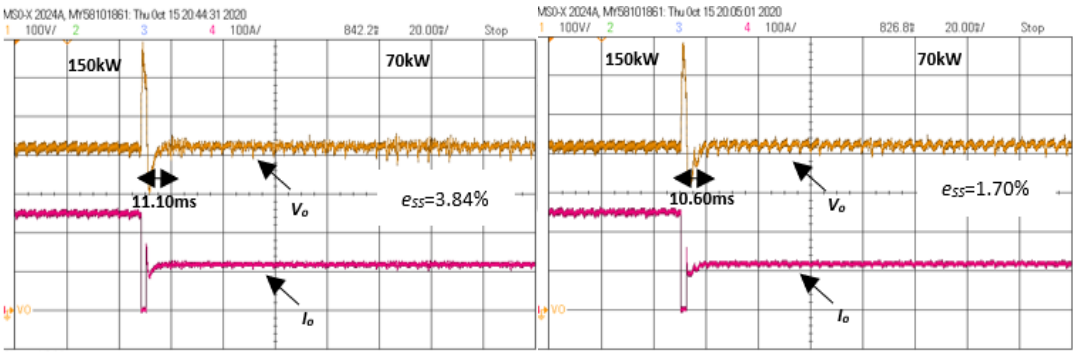

(a) (b)

Figure 13. Output waveform when the load step-down from 150 kW to 70 kW at 420 V with k = 1.12 (a) OPSO-PI-OT (b) OPSO-PI-RT (V_o: 100 V/div, I_o: 100 V/div; Time: 20 ms/div).

In summary, the comparative percentage of e_{SS} between OPSO-PI-RT and OPSO-PI-OT indicate that the OPSO-PI-RT has good accuracy with 14.65% superior performance than OPSO-PI-OT. Thus, by updating the K_P and K_I optimal values for current system conditions has diminished the ripple in the DAB system and guarantees the proposed OPSO-PI-RT is more precise than OPSO-PI-OT in both load step conditions. It proves that the K_P and K_I obtained in this method change according to the new load and ensure better performance of the DAB system with minimal e_{SS}.

5.2. Dynamic response performance

The DAB converter was further analyzed by measuring the dynamic response in terms of settling time during the disturbances or step changes in the system. The settling time for OPSO-PI-OT was longer, taking 15.80 ms for the V_o to reach desired value compared to OPSO-PI-RT with 15.60 ms during the load change from 100 kW to 200 kW at 270 V as shown in Figure 10. From Figure 11, the OPSO-PI-OT recorded the settling time of 13.20 ms to regulate back to the desired value after the load change at 375 V, which was 0.5 ms faster than OPSO-PI-OT.

Furthermore, when the load was changed from 150 kW to 70 kW at 270 V, as demonstrated in Figure 12, it is visibly shown that OPSO-PI-RT gives 0.45 ms faster recovery during transient than OPSO-PI-OT by producing 10.05 ms of settling time. Besides, the settling time of OPSO-PI-RT was shorter compared to OPSO-PI-OT as shown in Figure 13, where the settling time was 11.10 ms and 10.60 ms for OPSO-PI-OT and OPSO-PI-RT, respectively.

This evaluation will determine the speed of the controllers where it refers to the inversion of the settling time as shown in (10).

$$speed(s^{-1}) = \frac{1000}{settling\ \ time\ (ms)} \tag{10}$$

As predicted, the proposed OPSO-PI-RT achieved the best speed even after going through the reset process during the step change or disturbance by producing 85.28 s^{-1} compared to OPSO-PI-OT with 85.10 s^{-1}. The re-tuning in OPSO-PI-RT proved that it does not get distracted nor does it delay the system, and yet can still yield faster control than OPSO-PI-OT.

6. Conclusions

This paper proposed a bidirectional DAB DC-DC converter using SPS modulation. A 200 kW system with online auto-tuned PI using PSO algorithm was developed to improve system accuracy and improve the controller's speed. The main analyses, including CHIL results, were discussed for step change load disturbance at different voltage conversion ratios. The performance of the proposed OPSO-PI-RT method was compared with OPSO-PI-OT. The effectiveness of the proposed OPSO-PI-RT method was verified through CHIL experiments. It recorded least e_{SS} of less than 4% in all conditions tested. The proposed OPSO-PI-RT exhibited the faster dynamic response with minimal settling time in regulating back to the desired value after experiencing step change or disturbances in the DAB system. With the noteworthy outcomes of high accuracy and high speed that the proposed controller realized, both features are being expected to give the better performance of high power EV charger application. With these improvements, the EVs will receive significant consideration from users as the charger technology would feature rapid charging and fast system response by maintaining its system accuracy.

Acknowledgments

The authors would like to thank the University Malaysia Pahang for providing financial support under an internal research grant (Grant Number: RDU220309).

Conflict of interest

All authors declare no conflicts of interest in this paper.

References

1. Bose BK (2010) Global warming: Energy, Environmental Pollution, and the Impact of Power Electronics. *IEEE Ind Electron Mag* 4: 6–17. https://doi.org/10.1109/MIE.2010.935860
2. Khan SA, Islam R, Guo Y, Zhu J (2019) A New Isolated Multi-Port Converter With Multi-Directional Power Flow Capabilities for Smart Electric Vehicle Charging Stations. *IEEE T Appl Supercon* 29: 1–4. https://doi.org/10.1109/TASC.2019.2895526
3. Latifi M, Rastegarnia A, Khalili A, Sane S (2018) Agent-Based Decentralized Optimal Charging Strategy for Plug-in Electric Vehicles. *IEEE T Ind Electron* 66: 3668–3680. https://doi.org/10.1109/TIE.2018.2853609
4. Richardson DB (2013) Electric vehicles and the electric grid : A review of modeling approaches , Impacts , and renewable energy integration. *Renew Sustain Energy Rev* 19: 247–254. https://doi.org/10.1016/j.rser.2012.11.042
5. Rubino L, Capasso C, Veneri O (2017) Review on plug-in electric vehicle charging architectures integrated with distributed energy sources for sustainable mobility. *Appl Energy* 207: 438–464. https://doi.org/10.1016/j.apenergy.2017.06.097
6. Ashique RH, Salam Z, Aziz MJ, Bhatti AR (2017) Integrated photovoltaic-grid dc fast charging system for electric vehicle : A review of the architecture and control. *Renew Sustain Energy Rev* 69: 1243–1257. https://doi.org/10.1016/j.rser.2016.11.245
7. Blech T (2019) CHAdeMO DC charging standard: evolution strategy and new challenges.
8. Tan KM, Ramachandaramurthy VK, Yong JY (2016) Integration of electric vehicles in smart grid : A review on vehicle to grid technologies and optimization techniques. *Renew Sustain Energy Rev* 53: 720–732. https://doi.org/10.1016/j.rser.2015.09.012
9. Sha D, Wang X, Chen D (2017) High-Efficiency Current-Fed Dual Active Bridge DC – DC Converter With ZVS Achievement Throughout Full Range of Load Using Optimized Switching Patterns. *IEEE T Power Electron* 33: 1347–1357. https://doi.org/10.1109/TPEL.2017.2675945
10. Oggier GG, Garcia GO, Oliva AR (2009) Switching Control Strategy to Minimize Dual Active Bridge Converter Losses. *IEEE T Power Electron* 24: 1826–1838. https://doi.org/10.1109/TPEL.2009.2020902
11. Waltrich G, Hendrix MA, Duarte JL (2015) Three-Phase Bidirectional DC / DC Converter With Six Inverter Legs in Parallel for EV Applications. *IEEE T Ind Electron* 63: 1372–1384. https://doi.org/10.1109/TIE.2015.2494001
12. Karthikeyan V, Gupta R (2017) Light-load efficiency improvement by extending ZVS range in DAB- bidirectional DC-DC converter for energy storage applications. *Energy* 130: 15–21. https://doi.org/10.1016/j.energy.2017.04.119
13. De Doncker RW, Divan DM, Kheraluwala MH (1991) A Three-phase Soft-Switched High-Power-Density DC/DC Converter for High Power Applications. *IEEE T Ind Appl* 27: 63–73. https://doi.org/10.1109/28.67533
14. Zhang K, Shan Z, Jatskevich J (2017) Large- and Small-Signal Average-Value Modeling of Dual-Active-Bridge DC-DC Converter Considering Power Losses. *IEEE T Power Electron* 32: 1964–1974. https://doi.org/10.1109/TPEL.2016.2555929
15. Park Y, Chakraborty S, Khaligh A (2022) DAB Converter for EV Onboard Chargers Using

Bare-Die SiC MOSFETs and Leakage-Integrated Planar Transformer. *IEEE T Transp Electr* 8: 209–224. https://doi.org/10.1109/TTE.2021.3121172

16. Li L, Xu G, Xiong W, Liu D, Su M (2021) An Optimized DPS Control for Dual-Active-Bridge Converters to Secure Full-Load-Range ZVS With Low Current Stress. *IEEE T Transp Electr* 8: 1389–1400. https://doi.org/10.1109/TTE.2021.3106130
17. Deželak K, Bracinik P, Sredenšek K, Seme S (2021) Proportional-integral controllers performance of a grid-connected solar pv system with particle swarm optimization and ziegler–nichols tuning method. *Energies* 14: 2516. https://doi.org/10.3390/en14092516
18. Faisal SF, Beig AR, Thomas S (2020) Time Domain Particle Swarm Optimization of PI Controllers for Bidirectional VSC HVDC Light System. *Energies* 13: 866. https://doi.org/10.3390/en13040866
19. Hou N, Song W, Wu M (2016) Minimum-Current-Stress Scheme of Dual Active Bridge DC-DC Converter With Unified Phase-Shift Control. *IEEE T Power Electron* 31: 8552–8561. https://doi.org/10.1109/TPEL.2016.2521410
20. Shi H, Wen H, Chen J, Hu Y, Jiang L, Chen G, et al. (2018) Minimum-Backflow-Power Scheme of DAB-Based Solid-State Transformer With Extended-Phase-Shift Control. *IEEE T Ind Appl* 54: 3483–3496. https://doi.org/10.1109/TIA.2018.2819120
21. Shi H, Wen H, Hu Y, Jiang L (2018) Reactive Power Minimization in Bidirectional DC – DC Converters Using a Unified-Phasor-Based Particle Swarm Optimization. *IEEE T Power Electron* 33: 10990–11006. https://doi.org/10.1109/TPEL.2018.2811711
22. Hebala OM, Aboushady AA, Ahmed KH, Abdelsalam I (2018) Generic Closed Loop Controller for Power Regulation in Dual Active Bridge DC / DC Converter with Current Stress Minimization. *IEEE T Ind Electron* 66: 4468–4478. https://doi.org/10.1109/TIE.2018.2860535
23. Hassan M, Ge X, Woldegiorgis AT, Mastoi MS, Shahid MB, Atif R, et al. (2023) A look-up table-based model predictive torque control of IPMSM drives with duty cycle optimization. *ISA T.* https://doi.org/10.1016/j.isatra.2023.02.007
24. Xiong F, Wu J, Hao L, Liu Z (2017) Backflow Power Optimization Control for Dual Active Bridge DC-DC Converters. *Energies* 10: 1–27. https://doi.org/10.3390/en10091403
25. Tong A, Hang L, Li G, Jiang X, Gao S (2017) Modeling and Analysis of a DualActive-Bridge-Isolated Bidirectional DC/DC Converter to Minimize RMS Current With Whole Operating Range. *IEEE T Power Electron* 33: 5302–5316. https://doi.org/10.1109/TPEL.2017.2692276
26. Jaalam N, Ahmad AZ, Khalid AM, Abdullah R, Saad NM, Ghani SA, et al. (2022) Low Voltage Ride through Enhancement Using Grey Wolf Optimizer to Reduce Overshoot Current in the Grid-Connected PV System. *Math Probl Eng* 2022: 3917775. https://doi.org/10.1155/2022/3917775
27. Salman SS, Humod AT, Hasan FA (2022) Optimum control for dynamic voltage restorer based on particle swarm optimization algorithm. *Indonesian Journal of Electrical Engineering and Computer Science* 26: 1351–1359. https://doi.org/10.11591/ijeecs.v26.i3.pp1351-1359
28. Kumar R, Bansal HO, Gautam AR, Mahela OP, Khan B (2022) Experimental Investigations on Particle Swarm Optimization Based Control Algorithm for Shunt Active Power Filter to Enhance Electric Power Quality. *IEEE Access* 10: 54878–54890. https://doi.org/10.1109/ACCESS.2022.3176732
29. Borin LC, Mattos E, Osorio CR, Koch GG, Montagner VF (2019) Robust PID Controllers Optimized by PSO Algorithm for Power Converters. *2019 IEEE 15th Brazilian Power Electronics Conference and 5th IEEE Southern Power Electronics Conference, COBEP/SPEC,*

1–6. https://doi.org/10.1109/COBEP/SPEC44138.2019.9065642
30. Song W, Hou N, Wu M (2017) Virtual Direct Power Control Scheme of Dual Active Bridge DC – DC Converters for Fast Dynamic Response. *IEEE T Power Electron* 33: 1750–1759. https://doi.org/10.1109/TPEL.2017.2682982
31. Hassan M, Ge X, Atif R, Woldegiorgis AT, Mastoi MS, Shahid MB (2022) Computational efficient model predictive current control for interior permanent magnet synchronous motor drives. *IET Power Electron* 15: 1111–1133. https://doi.org/10.1049/pel2.12294
32. Zeng D, Zheng Y, Luo W, Hu Y, Cui Q, Li Q, et al. (2019) Research on Improved Auto-Tuning of a PID Controller Based on Phase Angle Margin. *Energies* 12: 1–16. https://doi.org/10.3390/en12091704
33. Sun X, Qiu J (2021) A Customized Voltage Control Strategy for Electric Vehicles in Distribution Networks with Reinforcement Learning Method. *IEEE T Ind Inform* 17: 6852–6863. https://doi.org/10.1109/TII.2021.3050039
34. Wang Y, Qiu D, Strbac G, Gao Z (2023) Coordinated Electric Vehicle Active and Reactive Power Control for Active Distribution Networks. *IEEE T Ind Inform* 19: 1611–1622. https://doi.org/10.1109/TII.2022.3169975
35. Ab-Ghani S, Daniyal H, Jaalam N, Ramlan NH, Saad NM (2022) Time-Variant Online Auto-Tuned PI Controller Using PSO Algorithm for High Accuracy Dual Active Bridge DC-DC Converter. *2022 IEEE International Conference on Automatic Control and Intelligent Systems, I2CACIS*, 36–41. https://doi.org/10.1109/I2CACIS54679.2022.9815470
36. Liu H, Song Q, Zhang C, Chen J, Deng B, Li J (2019) Development of bi-directional DC / DC converter for fuel cell hybrid vehicle. *J Renew Sustain Energy* 11: 44303. https://doi.org/10.1063/1.5094512
37. Yang J, Liu J, Zhang J, Zhao N, Wang Y, Zheng TQ (2018) Multirate Digital Signal Processing and Noise Suppression for Dual Active Bridge DC DC Converters in a Power Electronic Traction Transformer. *IEEE T Power Electron* 33: 10885–10902. https://doi.org/10.1109/TPEL.2018.2803744
38. Rodriquez A, Vazquez A, Lamar DG, Hernando MM, Sebastia J (2014) Different Purpose Design Strategies and Techniques to Improve the Performance of a Dual Active Bridge With Phase-Shift Control. *IEEE T Power Electron* 30: 790–804. https://doi.org/10.1109/TPEL.2014.2309853
39. Kennedy J, Eberhart R (1995) Particle Swarm Optimization. *Proc IEEE Int Conf Neural Networks* 4: 1942–1948.
40. Ishaque K, Salam Z, Shamsudin A, Amjad M (2012) A direct control based maximum power point tracking method for photovoltaic system under partial shading conditions using particle swarm optimization algorithm. *Appl Energy* 99: 414–422. https://doi.org/10.1016/j.apenergy.2012.05.026
41. Ishaque K, Salam Z, Amjad M, Mekhilef S (2012) An Improved Particle Swarm Optimization (PSO)– Based MPPT for PV With Reduced Steady-State Oscillation. *IEEE T Power Electron* 27: 3627–3638. https://doi.org/10.1109/TPEL.2012.2185713